Ocean Engineering 300 (2024) 117433

Contents lists available at ScienceDirect

Ocean Engineering

journal homepage: www.elsevier.com/locate/oceaneng

Research paper

Full Acoustic Analogy of the fluid-dynamics noise of an immersed cube

Giovanni Petris [*], Marta Cianferra [1], Vincenzo Armenio [1]

Dipartimento di Ingegneria e Architettura, Universitá degli Studi di Trieste, Piazzale Europa, 1, Trieste, 34127, Italy

ARTICLE INFO

Keywords:
FW-H
Wave equation
Underwater noise
FAA

ABSTRACT

The estimation of fluid dynamic noise generated by anthropogenic sources in realistic marine basins and on land is paramount for human safety and environmental protection. Classical acoustic analogies have limited capabilities when considering the natural variability and peculiarities of the acoustic propagation domain. The Full Acoustic Analogy (FAA), based on the combination of an acoustic analogy for source characterization and a propagation model for far-field transmission, allows the estimation of detailed soundmaps, practical when assessing the risk associated with exposure to fluid-dynamic noise, both impulsive and continuous. The verification of the methodology, consisting of comparing of the far-field acoustic pressure signal obtained with the FAA and with the Ffowcs-Williams and Hawkings equation (classical acoustic analogy for moving immersed bodies), is proven for the first time for the quadrupole non-linear terms. The latter may contribute significantly to the total noise field at small-to-medium distances from the source. In conjunction, the ability of the FAA method to predict the acoustic pressure distribution within the three-dimensional propagation domain is highlighted.

1. Introduction

Noise emissions compromise the environment and are a concern for both humans and wildlife. Prediction of flow-induced noise is necessary to mitigate the hazard associated with anthropogenic sources, like wind turbines or skyscrapers on land, propellers or pile-driving at sea, air and road traffic, and more. The development of numerical tools capable of predicting noise levels is valuable in the design phase of an infrastructure to evaluate both noise generation and propagation under conditions where physical experiments are challenging to perform. Also, concerning underwater radiated noise (URN), numerical tools can be exploited to assess the health status of the sea and predict future scenarios.

In this regard, the European Commission introduced the Marine Strategy Framework Directive (MSFD) to maintain the Good Environmental Status (GES). A recent official document (Borsani et al., 2023) prepared by the Technical Group on Underwater Noise (TG Noise), serves as a guiding framework for establishing European threshold values associated with continuous anthropogenic noise in water. This report builds upon the comprehensive efforts of recent EU projects like ACQUO, SONIC, JOMOPANS, NAVAIS, JONAS, SATURN, and QUIETSEAS. Traditional construction of sound maps in numerical models relies heavily on information regarding ship presence, size, and velocity acquired through the Automatic Identification System (AIS). Each ship signal is reconstructed using semi-empirical models, resulting in a point-like and omni-directional sound source (e.g., RANDI). These maps illustrate time-averaged noise levels and pertain solely to individual frequencies, potentially leading to a generalized underestimation of actual noise levels. Discussions and reports on such formulations have been extensively documented in deliverables and scientific journal articles linked to EU project activities, validating numerical data against experimental measurements (MacGillivray and de Jong, 2021). Yet, the modelling of complex sources like cavitating propellers remains a challenge within this framework. This limitation has been previously emphasized in the AQUO-SONIC guidelines (Baudin and Mumm, 2015; Borsani et al., 2023), and it continues to be an active area of research. In this context, it is necessary to refine large-scale acoustic mapping techniques that encompass multiple complex sources (such as ship propellers, offshore wind turbines, etc.) and can handle the propagation of acoustic waves under realistic conditions (i.e., incorporating significant effects of reflection and refraction).

An important class of numerical methods for the computation of flow-induced noise relies on the application of the acoustic analogy to fluid dynamics fields. These methods are defined as *hybrid* (Wang et al., 2006) since they decouple the computation of the turbulent fluid dynamic fields from the acoustic ones. Among the possible acoustic analogies that allow the computation of the acoustic pressure generated by immersed moving bodies there is the Ffowcs-Williams and Hawkings equation (FW-H) (Ffowcs Williams and Hawkings, 1969)

* Corresponding author.
E-mail addresses: giovanni.petris@phd.units.it (G. Petris), marta.cianferra@dia.units.it (M. Cianferra), vincenzo.armenio@dia.units.it (V. Armenio).
[1] These authors contributed equally to this work.

https://doi.org/10.1016/j.oceaneng.2024.117433
Received 15 December 2023; Received in revised form 23 February 2024; Accepted 7 March 2024

which has been extensively used for aeroacoustic applications first (see, for example (Brentner and Farassat, 2003; Ianniello, 2007; Mendez et al., 2013)) and subsequently for URN computation (see, among the others (Ianniello et al., 2013; Cianferra et al., 2019b; Cianferra and Armenio, 2021; Hu et al., 2021; Posa et al., 2022b,a)). The FW-H equation relies on the classical Lighthill theory and considers the presence of a noise-generator solid body immersed in the flow field.

A main limitation of the acoustic analogy is that the propagation is considered to occur in an infinite and homogeneous medium, given the use of the free-space Green function when solving the wave equation. However, this condition is not appropriate for real-life environmental applications characterized by geometric complexities and inhomogeneity in the fluid column. Tailored Green's functions are available for simple geometric configurations, such as the semi-infinite domain mimicking the presence of the free surface of the ocean (Goldstein, 1976) or regular perfectly-reflecting ducts, not suitable for open-sea scenarios. On the other hand, various methodologies have been developed to tackle the wave equation (see, among the others (Weinberg and Keenan, 1996; Sturm, 2005)). The majority of these approaches rely on frequency domain solutions, addressing far-field propagation in complex domains (for example accounting for inhomogeneous media). Such methodologies are suited for noise propagation from point-like sources which, therefore, do not exhibit directivity. Unfortunately this is not the case of fluid dynamic induced noise when the problem of noise propagation needs to be studied at small-to-intermediate distances from the source. In particular, several recent studies that have applied FW-H for characterizing propeller noise, pointed out its complex directivity, using the direct integration of the fluid dynamics fields (Cianferra et al., 2019b; Posa et al., 2022b; Posa, 2023) or the boundary element method (BEM) coupled with FW–H equation (Seol et al., 2002; Kim and Kinnas, 2022; Belibassakis and Prospathopoulos, 2023). Therefore, there is a need to develop methodologies able to overcome these limitations, specifically addressing complex noise sources characterized by a broadband spectrum and directivity, while also handling the propagation of acoustic waves in complex domains.

The Authors of the present paper have recently worked in the direction outlined above. Actually, in two successive papers the Authors have developed a numerical method for the propagation of noise generated by complex sources in a realistic environment: in Petris et al. (2022b) the Authors solved numerically the acoustic wave equation in the space–time domain considering simple sources and inhomogeneous media, characterized by the presence of waveguides; in Petris et al. (2022a), the Authors extended the method to consider the presence of complex sources. Specifically, the FW-H acoustic pressure computed at specific points in the 3D space was included as a forcing term into the propagation model, in order to predict the noise generated by a marine propeller in a confined domain.

At that stage of the research only the linear terms of the FW-H equation were considered (Petris et al., 2022a). However, it is well known in literature (see Cianferra and Armenio, 2021 for a discussion) that the wake of a body may contribute substantially to the composition of noise propagated at sea. Considering the noise generated by the wake (non-linear or quadrupole terms of the FW-H equation) is of crucial importance for a comprehensive analysis of fluid-dynamic noise. This is the issue accomplished in the present paper. Namely, starting from acoustic near-field computed with a classical acoustic analogy, it is possible to evaluate the propagation in arbitrary domains. The methodology, herein presented and named *Full Acoustic Analogy* (FAA) is general, in the sense that the choice of the model to characterize the source is arbitrary and related to the acoustic problem under investigation, and the choice of the propagation model can be also tailored to the characteristics of the domain.

Here we describe the complete methodology and validate it for the simple case of a bluff body immersed in a uniform flow. This geometry is archetypal of bodies moving at sea or placed in a steady current, with Reynolds and Mach numbers considered small compared to real marine applications. However, the only limitation to the practical use of the FAA with real-scale signals lies in the number of grid cells needed to replicate the entire frequency spectrum accurately, especially the high frequencies. Indeed, to propagate the high frequencies with a high degree of accuracy, the grid cells' dimensions must be reduced in accordance with the numerical scheme requirements. This aspect does not constitute a severe problem because the wave equation is hyperbolic, which enables the use of fast, time-marching numerical algorithms and high-performance parallel computers. The application of the acoustic analogy necessary to characterize the acoustic source needs high-fidelity CFD simulations of full-scale marine systems, which, to date, to the best of our knowledge, are not straightforward due to computational requirements. Instead, we may infer data from model scale simulations. In this case, using perfect similarity as suggested in Cianferra and Armenio (2021), the actual scale value of the Mach number can be considered, leaving just a scale effect on the Reynolds number. It should be noted that the generality of the methodology allows its application to atmospheric sound mapping.

The FAA verification is performed using the FW-H signal as a reference one, in the free-space case. The results show that this methodology is able to compute with a high degree of fidelity the noise propagation in the acoustic far-field, when compared with the direct FW-H computation.

This result enables the evaluation of flow-induced noise cases in a variety of complex propagation environments. For instance, in the case of a port, coastal area, or a sea channel where there are several continuous sources (e.g., propellers, wind turbines) along with submerged reflective obstacles (e.g., dams, canyons, mountainous structures), and water stratification.

In Section 2 we describe the theoretical approach of the FAA methodology, in Section 3 the case of the immersed cube is presented; in Section 4 we verify the FAA methodology and, finally, we give concluding remarks on the direction of future research in Section 5.

2. Full acoustic analogy

The FAA methodology allows the noise-source characterization and its signal propagation in heterogeneous and confined domains. It consists of three steps: an eddy-resolving numerical simulation of the flow around the immersed body solves the unsteady hydrodynamic field; the application of the acoustic analogy determines the acoustic near-field generated by the velocity and pressure fluctuations; the propagation model enables the transmission of the acoustic waves in the far-field. As discussed in the Introduction, an early and incomplete version of the methodology was first presented in Petris et al. (2022a), where it was applied to evaluate the noise generated by a marine propeller, limiting the analysis to the linear terms of the FW-H equation. In fact, in Petris et al. (2022a), we considered the linear terms of the FW-H equation only, thus neglecting the part of the noise emission associated with the quadrupole terms. In this article, we extend the methodology to the non-linear terms. In other words, we are now able to compute the propagation of the total noise generated by a submerged body, that is the aim of the research project as a whole.

Fig. 1 illustrates the three-step schematic of the FAA model, and these steps are separated, independent, and sequential. The inner square represents an eddy-resolving CFD simulation depicted as a flow around a body (a cube in this specific case). The Navier–Stokes equations need to be solved using an accurate eddy resolving methodology, since the quality of the fluid dynamic data is of paramount importance for the evaluation of the acoustic pressure. This aspect was also highlighted by Colonius and Lele (2004), Wang et al. (2006), who stated that fine-resolved unsteady CFD simulations must be performed to correctly capture the generation mechanism of noise, which limits the approach to DNS and LES compared to RANS. The latter may be employed when the generation mechanism is described by simple large-scale vortices.

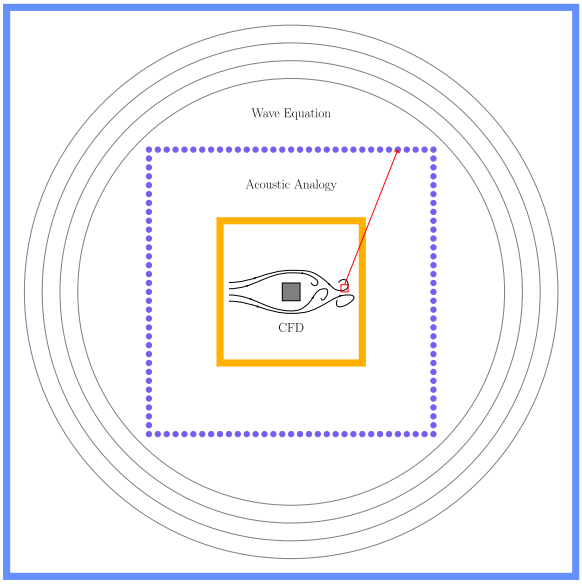

Fig. 1. Schematic of the FAA methodology.

In the second step, an acoustic analogy is employed to estimate the flow-induced noise. The generality of the methodology does not prescribe the use of a specific acoustic analogy. The aspect to be considered is that the chosen acoustic analogy must determine the noise emission on a cluster of microphones, posed at a certain distance so as to enclose the immersed body and its wake, see the square represented by blue dots in Fig. 1. In this work, we use the direct formulation of the FW-H equation (Section 2.1), which has been verified and employed in a number of recent papers (see Cianferra et al., 2018, 2019a,b and literature therein reported). The so-called porous formulation can also be used in this step.

The spatial layout of the microphone array over which the acoustic pressure is computed is arbitrary in the sense that any closed and convex shape can be used. For example, in Fig. 1, the acoustic pressure is evaluated over a square box at a certain distance from the body since the propagation model herein used solves the acoustic wave equation on a Cartesian grid, although rectangular or spherical distributions may also have been used. Alternatively, considering a propagation model based on cylindrical or spherical coordinates, the acoustic signal can be more effectively computed along microphones arranged in a cylindrical or spherical shape. Also, for the sake of convenience, the microphone's location may coincide with the grid points, considering the grid adopted in the third step. In this regard, it may be advantageous to first evaluate the frequency range of the acoustic source to establish an appropriate discretization for the propagation model. Subsequently, derive the microphone array accordingly.

Thus, as the best procedure to decide the microphone array placement, we stress that the FW-H signal serves two purposes: determining the microphone array width and the grid spacing of the propagation model. Low-frequency content is analysed for the former, while the high-frequency range rules the latter. In the case of the immersed cube presented in Section 3, the analysis of the FW-H spectra in the intermediate and far-field identifies that the energy caring frequencies are in the $10-20$ Hz range for both the linear and non-linear signals. Therefore, firstly, we identified a sufficient grid spacing for correctly propagating the acoustic waves in this specific range, and secondly, we identified a minimum number of microphones necessary to characterize the acoustic source based on the grid spacing. Note that the distance of the microphones from the source does not necessarily have to be the wavelength of the lowest frequency; it can be shorter, as in the present case. In this regard, we lack a specific criterion for this choice and continue investigating this aspect. Currently, the results of the tests conducted so far can still indicate that the microphone box must be sufficiently large (and refined) to capture the directivity of the signal. We observed that increasing the distance of the microphone array from the source and increasing the number of microphones employed to characterize the source provides more accurate solutions (Lamonaca et al., 2024). On the other hand, boxes that are too narrow around the source may overestimate the signal propagated with the wave equation. We can explain this as follows: FW-H generates a signal dominated by decays greater than $1/r$ in the near field, and if the microphones used to calculate FW-H are too close to the source, an overly intense signal is input into the propagation model, which may result in discrepancies between the FW-H and FAA signals. This problem is more pronounced in the case of rotating sources, for which a decay greater than $1/r^3$ is observed near the body. Lastly, we must balance computational complexity and practicality when choosing microphone distance and grid spacing.

In the third step of FAA, the FW-H signal is propagated considering an arbitrary domain, which may include reflective boundaries and variable density. The propagation model we adopted solves the acoustic wave equation on Cartesian uniform grids using the finite-difference method and it is introduced in Section 2.2.

The generality of the FAA methodology enables the study of various flow-induced noise problems, such as marine traffic noise (Petris et al., 2022a), wind farm noise, or noise generated by flow impacting a rigid object, as in the case presented in Section 3.1.

2.1. Ffowcs-Williams and Hawkings equation

The direct formulation of FW-H equation is generally adopted to evaluate the acoustic pressure generated by immersed moving bodies and unsteady flows, it reads as:

$$\begin{aligned}\hat{p}(\mathbf{x},t) = &\frac{\partial}{\partial t}\int_S \left[\frac{\rho v_i \hat{n}_i}{4\pi r|1-M_r|}\right]_\tau dS + \frac{1}{c_0}\frac{\partial}{\partial t}\int_S \left[\frac{\tilde{p}\hat{n}_i\hat{r}_i}{4\pi r|1-M_r|}\right]_\tau dS \\ &+ \int_S \left[\frac{\tilde{p}\hat{n}_i\hat{r}_i}{4\pi r^2|1-M_r|}\right]_\tau dS + \frac{1}{c_0^2}\frac{\partial^2}{\partial t^2}\int_W \left[\frac{T_{rr}}{4\pi r|1-M_r|}\right]_\tau dW \\ &+ \frac{1}{c_0}\frac{\partial}{\partial t}\int_W \left[\frac{3T_{rr}-T_{ii}}{4\pi r^2|1-M_r|}\right]_\tau dW + \int_W \left[\frac{3T_{rr}-T_{ii}}{4\pi r^3|1-M_r|}\right]_\tau dW,\end{aligned} \tag{1}$$

where $\tilde{p} = p - p_0$ denotes the pressure fluctuations over the surfaces with respect to the reference value p_0, $\hat{n}$ is the (outward) unit normal vector to the surface element dS, dW is the volume element, $T_{ij} = \rho u_i u_j + \left(\tilde{p} - c_0^2\tilde{\rho}\right)\delta_{ij}$ is the Lighthill tensor (considering the contribution of the viscous stress tensor negligible), ρ is the bulk density, and c_0 the speed of sound in the fluid, $r = |\mathbf{x}-\mathbf{y}|$ is the source-observer distance, being $\mathbf{x}$ the coordinate of the microphone and $\mathbf{y}$ the coordinate of the source element dS or dW, $\hat{r}_i$ is the i-component of the unit vector $(\mathbf{x}-\mathbf{y})/r$, τ is the emission time and t is the arrival time at the observer. $M_r = v_i\hat{r}_i/c_0 = 0$ is the local Mach number and $T_{rr} = T_{ij}\hat{r}_i\hat{r}_j$, while T_{ii} is the trace if the Lighthill tensor.

Eq. (1) computes the acoustic pressure at point $\mathbf{x}$ as the sum of pressure perturbations over the surfaces S and the flow contribution within the volume W. The surface integrals are defined as linear terms and represent the contribution of the moving solid boundaries to the noise. Note that for bodies at rest in a flow field, the velocity of the body surface is $v_i = 0$, thus the first term is neglected. The three volume integrals, referred to as the non-linear terms, evaluate the noise contribution associated to the unsteady flow field.

In Eq. (1) the integrals' kernel are computed at the emission time τ. This, in principle, differs from the signal's arrival time t at the observer. However, in some cases it is plausible to assume $t = \tau$. For instance, when the signal travels at a considerably higher speed compared to the source's motion or when the source's extension is much smaller

than the smallest wavelength. In these cases, the Maximum Frequency Parameter (MRF) (Cianferra et al., 2019a) is above $MRF > 1$ and the computation of the time delays can be neglected. These conditions were verified in the present case during the pre-processing phase, allowing to neglect the delay between t and τ.

2.2. Acoustic wave equation

The propagation model solves the acoustic wave equation, valid for the propagation of pressure waves in a fluid. It reads as:

$$\frac{1}{c(\mathbf{x})^2}\frac{\partial^2 p(\mathbf{x},t)}{\partial t^2} = \rho(\mathbf{x})\nabla\left(\frac{1}{\rho(\mathbf{x})}\nabla p(\mathbf{x},t)\right), \tag{2}$$

where $c(\mathbf{x})$ is the speed of sound of the medium, $p(\mathbf{x},t)$ is the acoustic pressure, $\rho(\mathbf{x})$ is the density of the medium. Eq. (2) is solved through a finite-difference method on a three-dimensional Cartesian grid with uniform spacing. An explicit scheme in employed, second-order accurate both in time and space. The details of the numerical approach and validation for point-like sources, such as monopole, dipole and quadrupole, are described in Petris et al. (2022b). The wave-propagation solver is currently an in-house code, developed using the Julia programming language (Bezanson et al., 2017). In order to mimic an unbounded domain, proper open-boundary conditions are implemented to avoid spurious reflections. Specifically, we adopt the Perfectly Matched Layer (PML) described in Chern (2019).

As mentioned above, the acoustic pressure originating from the unsteady flow is computed through the FW-H equation (Eq. (1)) over an array of microphones. The collection of these signals represents a time-varying Dirichlet boundary condition for Eq. (2). Note that this approach of imposing a forcing term at specific points is defined *hard-source* method. The *hard source* method is recognized for scattering any incoming waves, which may occur due to the presence of a secondary source or a reflective surface in the propagation domain. However, this scenario is not applicable to the case presented in this paper, as the cube is immersed in an infinite homogeneous domain. Nonetheless, to address the issue of spurious scattering, we have devised a new source-injection method, named the non-reflective hard source method (Lamonaca et al., 2024), based on the linearity of the wave equation. The new source-injection method enables the propagation of the acoustic waves in the confined domain, where the source is placed in the close vicinity of a reflecting surface, when obstacles are placed within the propagation domain, or when multiple sources are considered, without incurring in spurious reflection.

3. FAA signal construction

The acoustic analysis is carried out for a simplified bluff body immersed in a uniform current. The fluid-dynamic field was already analysed in Cianferra et al. (2018). Specifically, the Authors investigated the acoustic response of three simple geometries (sphere, cube, and prolate spheroid) using the standard acoustic analogy, assuming a homogeneous and unconfined medium. Among the possible geometries to be analysed, we chose the cube immersed in a constant flow since it produces an intense turbulent wake and, consequently, a non-negligible quadrupole signal. Indeed, both the turbulent wake (Fig. 2*b*), and the loads over the cube surface clearly contribute to the total noise. The cube is presented as a test case to verify the FAA methodology.

The acoustic results are presented in terms of Sound Pressure Level (SPL) or Spectrum Level (SL). The former is evaluated as $SPL = 20\log_{10}(p^{rms}/p_{ref})$, where p_{rms} is the root mean square of the acoustic pressure over a time window and p_{ref} is the pressure reference value, that, for underwater propagation, is equal to $p_{ref} = 10^{-6}$. While, the latter is defined as $SL = 20log_{10}(A/p_{ref})$, where A is the amplitude of the signal, evaluated applying the Fast Fourier Transform (FFT) of the time-varying acoustic pressure.

3.1. LES of an immersed cube

The cube is immersed in a flow having uniform velocity $U_0 = 0.5\,\mathrm{m/s}$. The side of the cube is $l_s = 0.008\,\mathrm{m}$ and the kinematic viscosity is $\nu = 1e{-}06\,\mathrm{m/s^2}$, giving a value of the Reynolds number based on the side of the cube $Re = l_s U_0/\nu = 4000$. The overall dimension of the numerical domain where the cube is immersed is $20l_s \times 20l_s \times 20l_s$ along the x, y, z direction respectively, where x is the streamwise direction and y and z are cross sectional directions. The centre of the cube is placed as shown in Fig. 2.

The constant flow at the inlet is obtained by imposing the prescribed uniform velocity, while a zero gradient boundary condition for the velocity and a fixed value for the pressure are set at the outlet. Slip condition is set to all lateral boundaries. The fluid dynamics fields were solved using OpenFOAM with an incompressible solver. We refer to the previous work (Cianferra et al., 2018) for further details.

The velocity and pressure fields, necessary for evaluating the FW-H acoustic pressure, have been collected every $0.3125l_s/U_0$ in a time window of $187.5l_s/U_0$. Note that, compared to the acoustic analysis conducted in Cianferra et al. (2018), we have extended the time window and increased the time interval between two consecutive data acquisitions. The latter does not affect the results since most of the acoustic energy is contained in the low-frequency range.

3.2. Near-field evaluation

The acoustic pressure is computed through Eq. (1) considering a suited array of microphones (box), as depicted in Fig. 3. The side of the box is $750\,l_s$ (6 m) and the distance between two successive microphones is set to $62.5l_s$ (0.5 m) in each direction. Note that the box side is very large compared to the size of the immersed cube. This is due to the fact that significant wavelengths of the acoustic pressure are much larger than the fluid dynamic characteristic length scale. The surface integrals are performed over the sides of the cube (S in Eq. (1)) and the volume integrals are performed over a cylindrical volume (W in Eq. (1)) with radius $R = 4\,l_s$, aligned with the wake axis. The cylinder starts at $x = -4\,l_s$ and reaches $x = 10\,l_s$, enclosing a significant part of the turbulent wake. The FW-H equation has been evaluated with an in-house post-processing utility developed within the OpenFOAM environment. Further details of the method are reported in Cianferra et al. (2019a).

Spectrum level of FW-H linear terms and the FW-H non-linear terms are shown in Fig. 4, evaluated at a microphone location $(375l_s, 0, 0)$. The highest peak observed corresponds to the frequency ~8 Hz. We adopted this as a reference frequency, meaning that the associated wavelength $\lambda_{8\ \mathrm{Hz}} = 23437.5\,l_s$ (187.5 m) is utilized to establish the domain size and to non-dimensionalize all quantities.

The maximum frequency evaluated is 100 Hz, limited by the sampling interval of the CFD simulation. Consequently, the minimum wavelength observed is $0.08\lambda_{8\ \mathrm{Hz}}$(15 m). The domain where the acoustic waves propagate needs to be large enough to capture the development of long waves, while grid spacing needs to satisfy the minimum requirement for a second order FDTD method, which is of 8 grid points for wavelength (Dablain, 1986). As a consequence, the grid spacing for the propagation method is adjusted accordingly and do not necessarily align with the fluid dynamics mesh. In particular, the spacing of the acoustic grid is orders of magnitude larger than that of the CFD grid.

3.3. Far-field computation

The noise evaluated at specific microphones through Eq. (1), as described in the previous subsection, is used as a time-varying Dirichlet boundary condition when solving Eq. (2). The microphones are disposed along a cubic array, having side equal to $0.032\lambda_{8\ \mathrm{Hz}}$ (6 m), and located at the centre of the domain. The propagation domain is a box of size $2.12\lambda_{8\ \mathrm{Hz}}$ (400 m)×$0.52\lambda_{8\ \mathrm{Hz}}$ (100 m)×$0.52\lambda_{8\ \mathrm{Hz}}$ (100 m) (see Fig. 5),

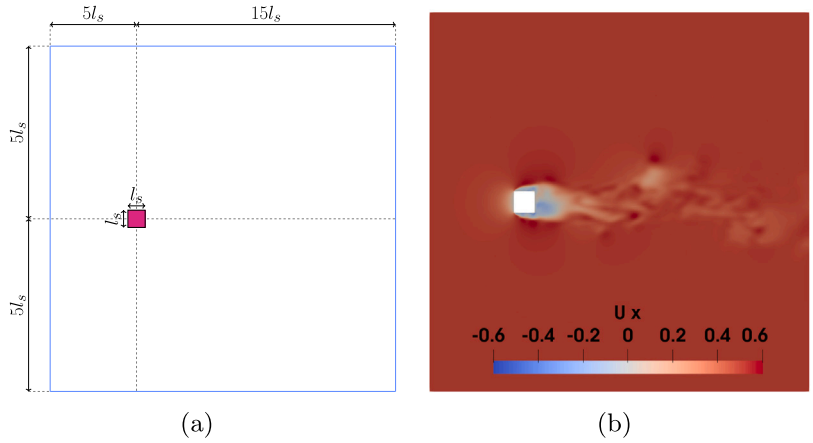

Fig. 2. (a) Schematic of the domain of the LES of the turbulent flow around the cube. See Cianferra et al. (2018) for more details. (b) Instantaneous streamwise velocity component over a longitudinal $(x-z)$ plane passing through the centre of the cube.

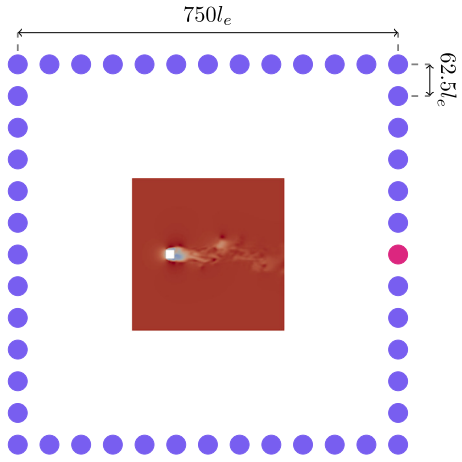

Fig. 3. Schematic of a section of the cubic array of microphones passing through the centre of the immersed cube. The figure at the centre is the CFD domain (enlarged). The microphone with a different colour positioned at $(375l_s, 0, 0)$ is used for the computation of the FFT and the acoustic pressure shown in Figs. 4 and 6.

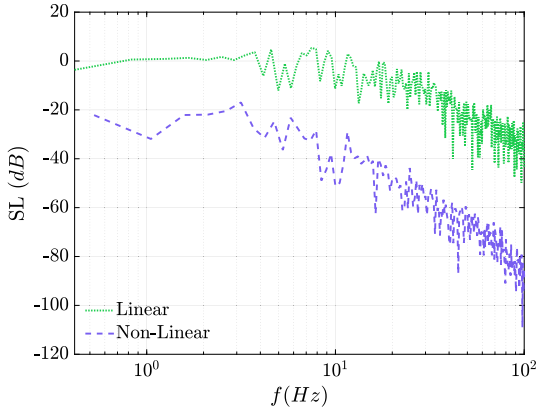

Fig. 4. Sound spectrum level (SL) of the linear terms and the non-linear terms of the FW-H equation evaluated at $(375l_s, 0, 0)$ for an interval of $150l_s/U_0$.

being the longest side parallel to the streamwise direction. The resolution of the numerical grid, which conforms to the spatial distribution of the microphones, is set to $\Delta x = \Delta y = \Delta z = 0.002\tilde{6}\lambda_{8\ \mathrm{Hz}}$ (0.5 m). Also, this resolution satisfies the accuracy requirement (Dablain, 1986) for correctly propagate acoustic waves with a frequency up to 200 Hz. The density of water is set to $\rho = 1000\,\mathrm{kg/m^3}$ and the speed of sound is $c = 1500\,\mathrm{m/s}$. The maximum allowable time step for the acoustic simulation is determined by the grid spacing and the speed of sound, and for stability reasons, it is set to $0.0119l_s/U_0$. Note that we store the flow field (instantaneous velocity and pressure fields) at fixed time intervals based on the maximum acoustic frequency we intend to propagate, avoiding unnecessary data storage. However, higher temporal resolution is needed when solving the wave equation for the stability requirements of the numerical method adopted; this leads to a time interpolation of the FW-H data. A solution to the data storage issue would be to solve the FW-H equation at each time step during the CFD experiment. In this case, the microphone positions required for applying the FAA methodology must be predetermined.

The time-interpolation of the FW-H data performed is shown in Fig. 6. We display the acoustic pressure at the microphone $(375l_s, 0, 0)$ in the time interval from $75l_s/U_0$ to $137.5l_s/U_0$, where we have labelled $FW-H$ the acoustic pressure obtained evaluating the FWH linear terms, and Wave the interpolated ones. This procedure does not affect the results since, at very high frequencies, there is no noteworthy acoustic energy. This procedure has also been done for the acoustic pressure of the FW-H non-linear terms (not shown).

In principle, the FW-H equation provides for the acoustic signal in the case of a source placed in an unbounded and homogeneous domain. Thus, we verify the accuracy of the FAA method by comparing the FW-H signal against the one obtained with the propagation model. For this purpose, all the external boundaries of the propagation domain have open-boundary conditions, enabling the acoustic waves to leave the domain without spurious reflections.

4. Verification of the FAA

In this Section, we compare the results obtained with the FW-H equation and with the FAA approach. We analyse both the linear and the non-linear terms, separately. The former was already verified in the case of a marine propeller (Petris et al., 2022a). The root-mean-square of pressure has been computed once the pressure has reached a statistically stable solution. This condition is fully met once the acoustic waves have crossed the furthest boundary of the numerical domain. In the next Sections 4.1 and 4.2, we analyse the decay of linear and non-linear terms, respectively, considering microphones distributed along a line passing through the centre of the body and parallel to the wake axis. The line is $1.06\lambda_{8\ \mathrm{Hz}}$ (200 m) long and the FW-H data are collected

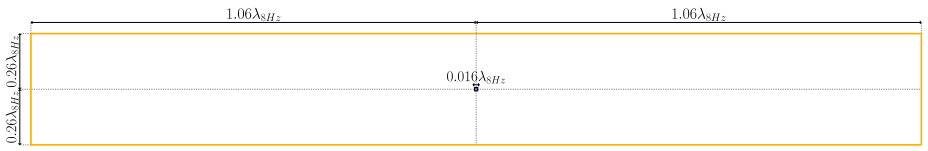

Fig. 5. Schematic of the propagation domain, where the space–time variation of the acoustic waves is evaluated with the acoustic wave equation. The rectangular cuboid is $2.12\lambda_{8\ \mathrm{Hz}}$ (400 m) long in the streamwise direction and has a square base $0.52\lambda_{8\ \mathrm{Hz}}$ (100 m) wide. The acoustic source evaluated with the FW-H equation is placed at the centre of the domain.

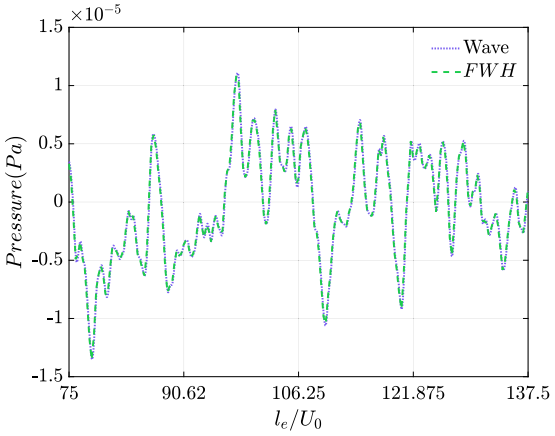

Fig. 6. Interpolation of the acoustic pressure of the linear terms of the FW-H equation at the microphone $(375l_s, 0, 0)$.

over 200 microphones positioned with a spacing of $0.0053\lambda_{8\ \mathrm{Hz}}$ (1 m). To further verify the results we show the acoustic pressure and the SL at the farthest microphone positioned at $1.06\lambda_{8\ \mathrm{Hz}}$ (200 m). Then, in order to check the accuracy of the FAA methodology in all directions we also compare the directivity patterns in Section 4.3. In order to compute the directivity, the FW-H data are collected at 200 microphones located on a circumference with a radius equal to $0.16\lambda_{8\ \mathrm{Hz}}$ (30 m). Instead, the acoustic pressure evaluated with the propagation model is available on a Cartesian grid, thus, a bilinear interpolation was performed to extract the data at the same location.

4.1. Decay of FW-H linear terms

We evaluate the decay of the acoustic pressure in the far-field, the latter being considered as the distance r for which $kr > 1$. In the present case, we have considered as a reference wavelength k the principal frequency of the linear term observed at the microphone $(375l_s, 0, 0)$, thus $k = 2\pi/\lambda_{8\ \mathrm{Hz}}$.

The decay with the distance of the second linear term S^2 and third linear term S^3 is shown in Fig. 7 in terms of Sound Pressure Level (SPL). The decay rates $1/r$ and $1/r^2$ are visible for the S^2 and S^3 terms, respectively. Accordingly, we observe that S^3 is more intense near the source, whereas S^2 becomes predominant at intermediate-to-large distances. This aspect is evident in Fig. 8, where we present the comparison between the FAA signal and the FW-H signal, both obtained by considering the sum of S^2 and S^3.

The S^2 term becomes predominant at $\sim 0.1\lambda_{8\ \mathrm{Hz}}$ (18.75 m). The results of the FAA methodology shows the correct decay and slightly overestimate the results obtained with the FW-H model. Specifically, the maximum difference observed is ~0.5 dB, recorded at a distance $1.06\lambda_{8\ \mathrm{Hz}}$ (200 m)

In order to investigate on the correct far-field transmission of the time-signal computed through the FAA methodology we compare in Fig. 9 the acoustic pressure evaluated at the farthest microphone located at $(1.06\lambda_{8\ \mathrm{Hz}}, 0, 0)$ (200 m, 0, 0), using the two methods. The resulting signal from FAA (labelled Wave) matches almost perfectly the FW-H results. We only observe a slight overestimation of the amplitude in correspondence of the higher peaks, which, as a consequence, was observed also in the SPL value (Fig. 8).

The comparison is also carried out by observing the frequency content, in Fig. 10. The SL obtained with the FAA exhibits a slight overestimation above 30 Hz compared to the FW-H results. These minor differences may stem from the time-interpolation of the source signals, which is conducted as a necessary step to process the FW-H data before loading it into the propagation model. Indeed, in Fig. 6, where the hard-source signals are represented, the values obtained with the FFA method (labelled Wave) are slightly higher with respect to the FW-H acoustic pressure. The difference is then retained in the far field. Clearly, such an error can be avoided by sampling the CFD data with smaller time steps.

The verification of the linear part of the FAA methodology in the case of an immersed body at rest proves that the FAA methodology is reliable in propagating the overall pressure constituted by the sum of linear terms of the FW-H equation.

4.2. Decay of FW-H non-linear terms

In this section, the FAA methodology is verified for the non-linear terms of the FW-H equation. This second step constitutes a more delicate part of the methodology because the non-linear part exhibits a quadrupole directivity. Actually, in the case of rotating sources, the acoustic field may present additional complexities. In general, we could say that the FAA methodology is sensitive to sources giving rise to complex acoustic patterns. The main issue is related to the nesting of FW-H data as a forcing term in the propagation model. Indeed, to accurately capture the source signal transmission in all directions, a refined and large enough array of microphones is needed.

The decay of the non-linear terms of the FW-H equation is analysed in Fig. 11. As expected, the three non-linear terms exhibit a different decay. The third term, which has the higher value of SPL near the source, decays very rapidly as $1/r^3$. Thus, its contribution is negligible in the far field. The other two terms have lower value of SPL near the source; however, since the decay rate is lower, $1/r^2$ for the second term and $1/r$ for the first term, their contribution to the overall acoustic level in the far field is more relevant. Note that at the intermediate field, of great importance for practical applications, the three contributions are comparable. Also, we refer to the recent study (Ianniello, 2016) where different decays are observed for a rotating source.

The decay of the total SPL originating from the sum of FW-H non-linear terms is shown in Fig. 12. We observe that there is a sharp transition of the SPL decay at $\sim 0.35\lambda_{8\ \mathrm{Hz}}$ (66 m): the $1/r^3$ decay, important in the near field, turns into the $1/r$ decay in the far field. In this case, a clear decay of the second order $1/r^2$ is not observed. The results clearly display a good agreement between the FAA methodology (Wave) and the FW-H model. We observed a maximum overestimation of the SPL evaluated with the FAA of about 0.3 dB at $1.06\lambda_{8\ \mathrm{Hz}}$ (200 m) compared to the SPL evaluated with FW-H equation, at the farthest microphone considered.

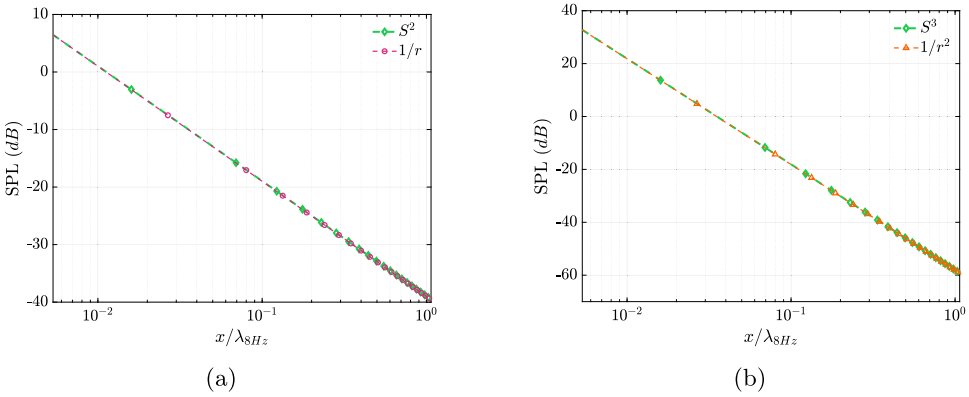

Fig. 7. SPL decay along a line of length $1.06\lambda_{8\ \mathrm{Hz}}$ (200 m) passing through the centre of the body in the direction of the wake: (a) second linear term S^2 of the FW-H equation; (b) third linear term S^3 of the FW-H equation.

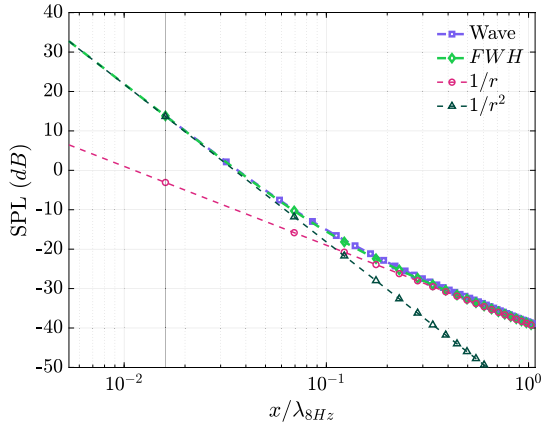

Fig. 8. Comparison of the SPL decay of the linear surface terms of the FW-H along a line of length $1.06\lambda_{8\ \mathrm{Hz}}$ (200 m) passing through the centre of the body in the direction of the wake with the acoustic pressure obtained with the FAA methodology ($Wave$).

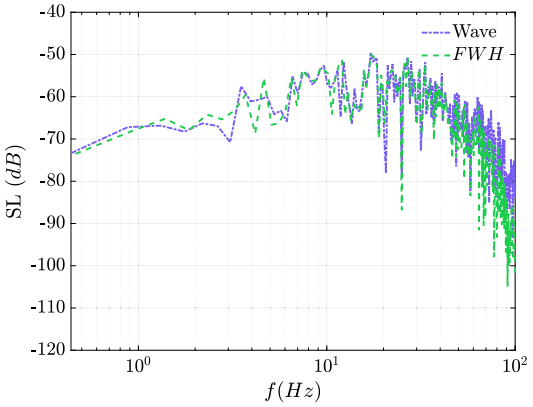

Fig. 10. SL of the acoustic pressure obtained with the FAA methodology (Wave) and the FW-H equation in a time interval of $150 l_s/U_0$ at the point $(1.06\lambda_{8\ \mathrm{Hz}}, 0, 0)$ of the linear surface terms of the FW-H equation.

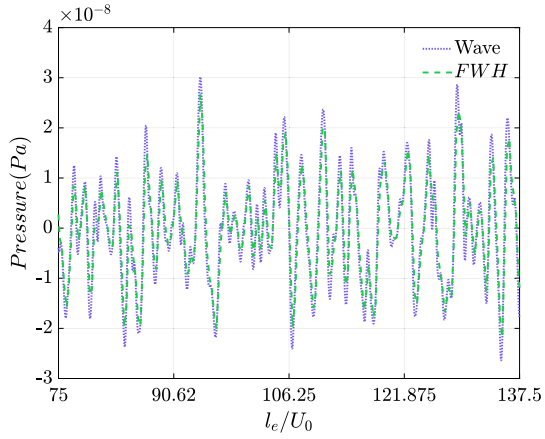

Fig. 9. Acoustic pressure of the linear surface terms of the FW-H equation measured at $(1.06\lambda_{8\ \mathrm{Hz}}, 0, 0)$ with the FAA (Wave) and the FW-H approach in the time window $75 - 137.5\, l_s/U_0$.

The overestimation is evident when looking at the time–history of the acoustic pressure: in Fig. 13 we report the acoustic signal computed at location $(1.06\lambda_{8\ \mathrm{Hz}}, 0, 0)$. As for the linear case (Fig. 10), we observe that the peak values of acoustic pressure evaluated with the FAA methodology are slightly higher than those obtained with the FW-H equation. We attribute this error to the time-interpolation of the FW-H data. Apart from this minor difference, the FAA methodology replicates accurately the signal computed with the FW-H equation.

Fig. 14 shows the spectrum of the signal presented in the previous Fig. 13. As for the linear part, some differences are observed at high frequency range, to be attributed to the interpolation procedure discussed above.

To summarize, we have demonstrated that the FAA methodology accurately predicts the decay of the sound pressure level of the FW-H non-linear terms in the intermediate-to-far field. This result is essential since, in a broad class of practical environmental and engineering applications, the non-linear terms can contribute quite significantly to the overall acoustic pressure; this is true typically in the acoustic near field or along specific directions in the far field where the linear (dipole) terms are less efficient in propagating the acoustic pressure.

4.3. Directivity patterns

The last section presents the directivity profiles, evaluated with the two methodologies: FW-H versus FAA. This analysis is conducted to ensure that the FAA methodology can correctly resolve the noise propagation in the three-dimensional space and not just along preferential directions. We limit the analysis to the plane parallel to the streamwise direction and normal to the cross-stream direction. This choice is driven by the symmetry of the fluid-dynamics fields and the resulting acoustic fields

We present the directivity obtained considering linear terms and non-linear terms of the FW-H equation separately. In the following

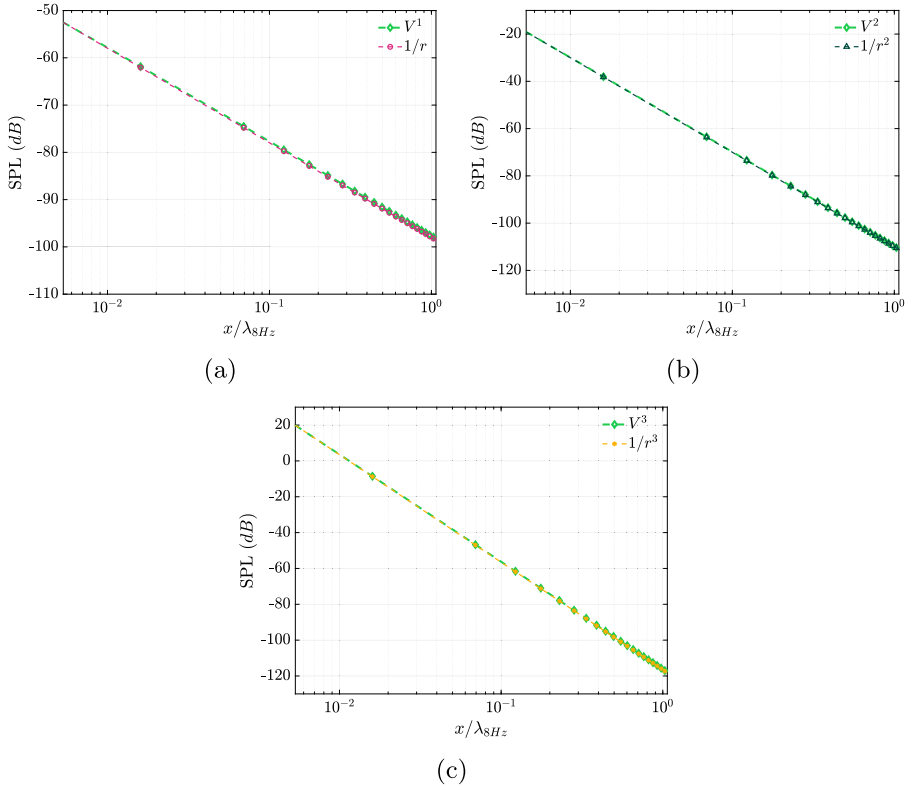

Fig. 11. SPL decay along a line of length $1.06\lambda_{8\ \mathrm{Hz}}$ (200 m) passing through the centre of the body in the direction of the wake: (a) first non-linear term V^1; (b) second non-linear term V^2; (c) third non-linear (volume) term V^3 of the FW-H equation (1).

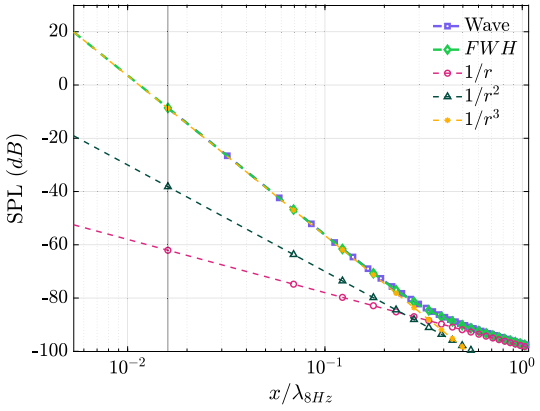

Fig. 12. Comparison of the SPL decay of the non-linear volume terms of the FW-H along a line of length $1.06\lambda_{8\ \mathrm{Hz}}$ (200 m) passing through the centre of the body in the direction of the wake obtained with the FAA methodology (Wave) and the FW-H equation.

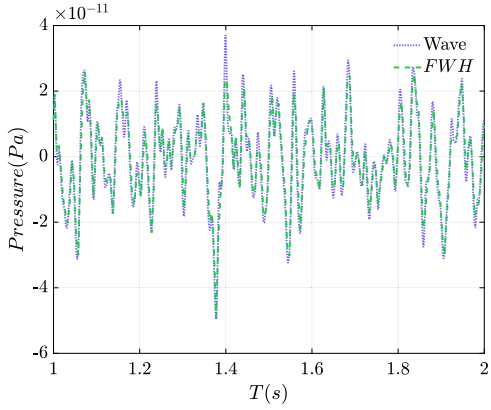

Fig. 13. Acoustic pressure of the non-linear volume terms of the FW-H equation measured at $(1.06\lambda_{8\ \mathrm{Hz}}, 0, 0)$ with the FAA (Wave) and the FW-H approach in the time window $75 - 137.5\, l_s/U_0$.

plots, the wake direction is at angle 0° and all the p_{rms} values are computed in a time interval $150 l_s/U_0$.

Fig. 15(a) shows the directivity plot of the linear terms at different radii evaluated through the FW-H equation, and Fig. 15(b) shows the comparison between the two approaches at the farthest radius $r = 0.16\lambda_{8\ \mathrm{Hz}}$ (30 m). As expected, a dipole-like pattern is observed: the directivity plot shows that more acoustic energy is propagated in the crosswise direction than in the streamwise direction. This behaviour is naturally observed at all radii, the main difference being that as the distance from the source increases, the relative difference between the maximum and minimum p_{rms} value decreases, so the dipole-like pattern is partially lost at the far-field (Fig. 15a).

We also observe a slight inclination of the dipole axis, likely attributed to the flow behaviour assumed during the considered time interval. In particular, the fluid dynamic loads on the cube's sides, responsible for the linear terms' outcomes, are unevenly distributed in time. This suggests that a large time window is needed to obtain a complete symmetrical field. Also, using advanced techniques to evaluate the stationarity the fluid dynamics fields is advisable for future analysis, such as the transient scanning technique (Brouwer et al., 2019). Overall, the results obtained with the FAA method differ from the FW-H outcomes by less than 0.1×10^{-7} Pa (1 dB), and similar directivity pattern is observed (Fig. 15b).

The directivity of the non-linear terms exhibits the typical quadrupole shape at all the radii (Fig. 16a). In this case, the quadrupole has two pronounced lobes along the streamwise direction and two

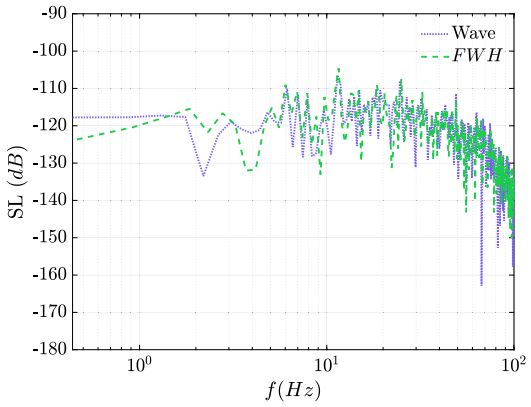

Fig. 14. SL of the acoustic pressure obtained with the FAA methodology ($Wave$) and the FW-H equation in a time interval of $150 l_s/U_0$ at the point $(1.06\lambda_{8\ \mathrm{Hz}}, 0, 0)$ for the non-linear volume terms of the FW-H equation.

minor lobes in the cross-stream direction. This effect can be associated with the fluid flow structure present in the wake, stretched along the streamwise direction. This feature is observed at all the radii, and compared to the linear terms (Fig. 15a), there is less difference in the relative amplitude between the maximum and the minimum value of the p_{rms}. Therefore, the non-linear terms maintain the same directivity at a farther distance compared to the linear terms. We note that the variation in the directivity pattern may depend on the dominance of one term over the others, which changes with distance. Notably, in the very far field, terms decaying as $1/r$ will prevail, accounting for the spherical symmetry attained at extremely long distances. Also in this case the p_{rms} evaluated with the FAA methodology (Wave) is in agreement with that evaluated with the FW-H equation (Fig. 16b) at the outermost radius $r = 0.16\lambda_{8\ \mathrm{Hz}}\,(30\,\mathrm{m})$. The results show that the FAA method slightly overestimates the maxima and underestimates the minima compared to the FW-H equation. The maximum difference is less than 0.2×10^{-7} Pa.

The ability to simultaneously compute the pressure distribution on an extended domain is one of the advantages of the FAA method. Indeed, instead of computing the acoustic pressure on a discrete set of microphones, we quickly access acoustic data over three-dimensional domain. Therefore, it is possible to create isosurfaces of the acoustic pressure to estimate the 3D-directivity patterns of the propagating waves. This aspect is of great importance to evaluate the direction in which the majority of the acoustic pressure is emitted by the source and for the individualization of any symmetry of the pressure distribution.

Fig. 17(a) shows the isosurface $p_{rms} = 1e^{-06}$ of the linear terms, obtained through the FAA method. As expected, the acoustic field is axial-symmetric. Namely, the spheroid has the same diameter along both the Y and Z directions. In the streamwise direction, an inflection of the surface is observed, with the minimum along the line $(x, 0, 0)$, which is the one passing through the cube centre. This inflection corresponds to the minimum of the dipole-like directivity observed in Fig. 15.

Fig. 17(b) shows the isosurface $p_{rms} = 1e^{-08}$ of the non-linear terms, obtained through the FAA method. The quadrupole-like shape is resembled, stretched along the streamwise direction (x), as visible in Fig. 16.

5. Conclusions

This study marks the last work introducing the Full Acoustic Analogy (FAA), a methodology designed and developed to study the propagation of sound from fluid dynamic sources. By overcoming established limitations of classical acoustic analogies, this approach provides a comprehensive framework. Typically, flow-induced noise from moving immersed bodies is computed using the FW-H equation, delineating two distinct contributions to the total acoustic pressure. The first arises from the flow-displacement due to the body motion and pressure fluctuations on the body surface (linear terms), while the second results from the unsteady fluid-dynamics fields in the developing wake behind the bodies (non-linear terms). The propagation of the latter with the FAA was evaluated and verified for the case of an immersed body (cube) in a uniform flow.

The verification entails a comparison between the FW-H equation and the FAA methodology concerning the propagation of noise generated by the immersed body. The analysis explores both linear and non-linear terms, emphasizing how the novel FAA methodology accurately propagates acoustic pressure at various distances from the noise source, matching the signal resulting from the FW-H equation. These findings not only validate the FAA but also underscore its ability to precisely model acoustic pressure distribution within a three-dimensional domain.

The implications of these results are far-reaching, offering a promising avenue for evaluating the propagation of noise generated by anthropogenic sources (e.g., wind turbines, propellers, pile driving) within complex and realistic environments. The latter encompass reflective surfaces, the presence of multiple sources, and fluid column stratification. Specifically, this methodology fits as a possible means of

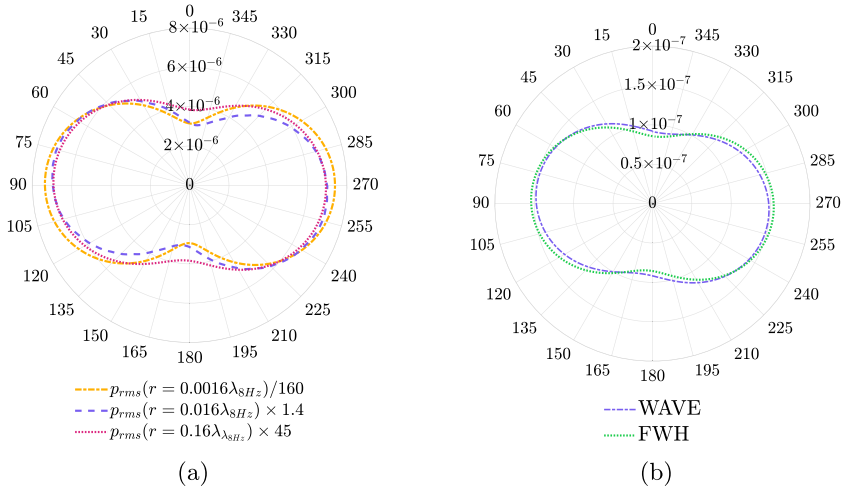

Fig. 15. (a) Comparison of the p_{rms} evaluated with the FWH equation at three different radii. (b) Comparison of the p_{rms} evaluated with the FAA methodology (Wave) and the FW-H equation of the linear surface terms of the FW-H equation over a circumference with radius $r = 0.16\lambda_{8\ \mathrm{Hz}}\,(30\,\mathrm{m})$. The inlet is at an angle equal to 180°.

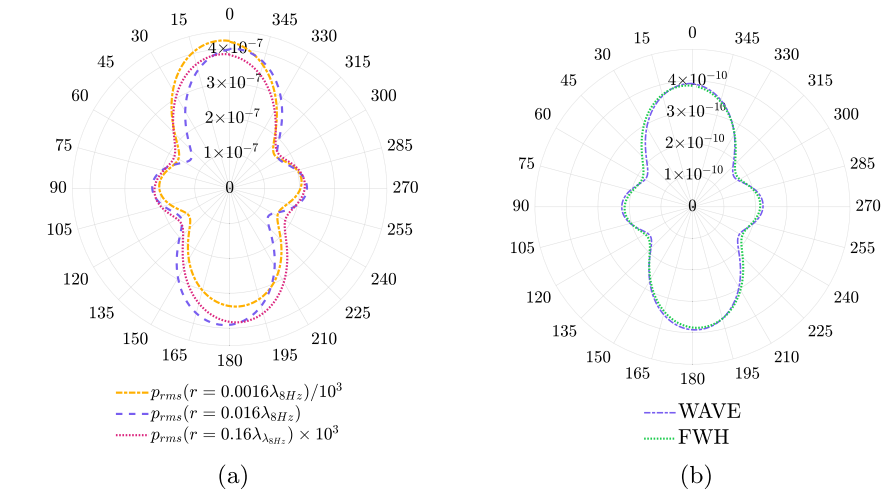

Fig. 16. (a) Comparison of the p_{rms} evaluated with the FWH equation at three different radii. (b) Comparison of the p_{rms} evaluated with the FAA methodology (Wave) and the FW-H equation of the non-linear volume terms of the FW-H equation over a circumference with radius $r = 0.16\lambda_{8\ \mathrm{Hz}}$ (30 m). The inlet is at an angle equal to 180°.

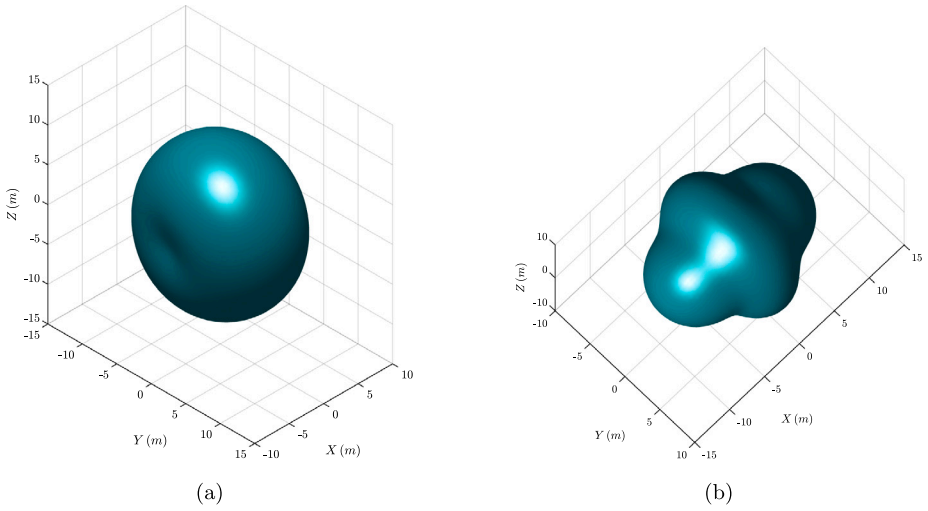

Fig. 17. Isosurface of p_{rms} of the linear terms of the FWH ($p_{rms} = 1e{-}06$) (a) and of the non-linear terms of the FWH ($p_{rms} = 1e^{-08}$) computed with the FAA method.

investigation for constructing detailed basin-scale acoustic maps, capturing real-time temporal acoustic field signals. Coastal and harbour areas, protected zones, sites with intense maritime traffic, or locations near offshore wind farms could be considered for examination.

CRediT authorship contribution statement

Giovanni Petris: Writing – original draft, Software, Methodology, Conceptualization. **Marta Cianferra:** Writing – review & editing, Supervision, Funding acquisition. **Vincenzo Armenio:** Writing – review & editing, Supervision, Methodology, Funding acquisition.

Declaration of competing interest

The authors declare that they have no known competing financial interests or personal relationships that could have appeared to influence the work reported in this paper.

Data availability

Data will be made available on request.

Acknowledgements

This research is part of the project SONORA "Filling the gap: Thresholds assessment and impact beyond acoustic pressure level linked to emerging blue-growth activities", project under the *JPI Oceans (2022), Joint call for proposals: Underwater Noise in the Marine Environment*, and has received financial support from MUR (Ministero dell'Università e della Ricerca) with the identifier CUP J93C22001730001. The authors acknowledge the support of the Center of Advanced Computing and Modelling at the University of Rijeka for providing the computing resources.

References

Baudin, E., Mumm, H., 2015. Guidelines for regulation on UW noise from commercial shipping (SONIC deliverable 5.4). Achieve Quieter Oceans by Shipping Noise Footprint Reduction, FP7-Grant Agreement No.

Belibassakis, K., Prospathopoulos, J., 2023. A 3d-BEM for underwater propeller noise propagation in the ocean environment including hull scattering effects. Ocean Eng. 286, 115544. http://dx.doi.org/10.1016/j.oceaneng.2023.115544.

Bezanson, J., Edelman, A., Karpinski, S., Shah, V.B., 2017. Julia: A fresh approach to numerical computing. SIAM Rev. 59 (1), 65–98. http://dx.doi.org/10.1137/141000671.

Borsani, J., Andersson, M., Andre, M., Azzellino, A., Bou, M., Castellote, M., Ceyrac, L., Dellong, D., Folegot, T., Hedgeland, D., Juretzek, C., Klauson, A., Leaper, R.,

Le Courtois, F., Liebschner, A., Maglio, A., Müller, A., Norro, A., Novellino, A., Outinen, O., Popit, A., Prospathopoulos, A., Sigray, P., Thomsen, F., Tougaard, J., Vukadin, P., Weilgart, L., Druon, J., Hanke, G., Casier, M., 2023. Setting EU Threshold Values for Continuous Underwater Sound KJ-04-23-492-EN-N (online). Publications Office of the European Union, Luxembourg (Luxembourg), http://dx.doi.org/10.2760/690123, (online).

Brentner, K.S., Farassat, F., 2003. Modeling aerodynamically generated sound of helicopter rotors. Prog. Aerosp. Sci. 39 (2–3), 83–120. http://dx.doi.org/10.1016/S0376-0421(02)00068-4.

Brouwer, J., Tukker, J., Klinkenberg, Y., van Rijsbergen, M., 2019. Random uncertainty of statistical moments in testing: Mean. Ocean Eng. 182, 563–576. http://dx.doi.org/10.1016/j.oceaneng.2019.04.068.

CEMIS/AC, DC.N.S. (Coordinator, France), 2012. ACQUO. URL http://www.aquo.eu/.

Chern, A., 2019. A reflectionless discrete perfectly matched layer. J. Comput. Phys. 381, 91–109. http://dx.doi.org/10.1016/j.jcp.2018.12.026.

Cianferra, M., Armenio, V., 2021. Scaling properties of the Ffowcs-Williams and Hawkings equation for complex acoustic source close to a free surface. J. Fluid Mech. 927, A2. http://dx.doi.org/10.1017/jfm.2021.723.

Cianferra, M., Armenio, V., Ianniello, S., 2018. Hydroacoustic noise from different geometries. Int. J. Heat Fluid Flow 70, 348–362. http://dx.doi.org/10.1016/j.ijheatfluidflow.2017.12.005.

Cianferra, M., Ianniello, S., Armenio, V., 2019a. Assessment of methodologies for the solution of the Ffowcs Williams and Hawkings equation using LES of incompressible single-phase flow around a finite-size square cylinder. J. Sound Vib. 453, 1–24. http://dx.doi.org/10.1016/j.jsv.2019.04.001.

Cianferra, M., Petronio, A., Armenio, V., 2019b. Non-linear noise from a ship propeller in open sea condition. Ocean Eng. 191, 106474.

Colonius, T., Lele, S.K., 2004. Computational aeroacoustics: Progress on nonlinear problems of sound generation. Prog. Aerosp. Sci. 40 (6), 345–416. http://dx.doi.org/10.1016/j.paerosci.2004.09.001.

Dablain, M.A., 1986. The application of high-order differencing to the scalar wave equation. Geophysics 51 (1), 54–66. http://dx.doi.org/10.1190/1.1442040.

Ffowcs Williams, J.E., Hawkings, D.L., 1969. Sound generation by turbulence and surfaces in arbitrary motion. Philos. Trans. R. Soc. Lond. Ser. A Math. Phys. Sci. 264 (1151), 321–342. http://dx.doi.org/10.1098/rsta.1969.0031.

Goldstein, M.E., 1976. Aeroacoustics. New York.

Hu, J., Ning, X., Zhao, W., Li, F., Ma, J., Zhang, W., Sun, S., Zou, M., Lin, C., 2021. Numerical simulation of the cavitating noise of contra-rotating propellers based on detached eddy simulation and the Ffowcs Williams–Hawkings acoustics equation. Phys. Fluids 33 (11), http://dx.doi.org/10.1063/5.0065456.

Ianniello, S., 2007. New perspectives in the use of the Ffowcs Williams–Hawkings equation for aeroacoustic analysis of rotating blades. J. Fluid Mech. 570, 79–127. http://dx.doi.org/10.1017/S002211200600293X.

Ianniello, S., 2016. The ffowcs Williams–Hawkings equation for hydroacoustic analysis of rotating blades. Part 1. The rotpole. J. Fluid Mech. 797, 345–388. http://dx.doi.org/10.1017/jfm.2016.263.

Ianniello, S., Muscari, R., Di Mascio, A., 2013. Ship underwater noise assessment by the acoustic analogy. Part I: nonlinear analysis of a marine propeller in a uniform flow. J. Mar. Sci. Technol. 18, 547–570. http://dx.doi.org/10.1007/s00773-013-0227-0.

Kim, S., Kinnas, S.A., 2022. Numerical prediction of propeller-induced noise in open water and ship behind conditions. Ocean Eng. 261, 112122. http://dx.doi.org/10.1016/j.oceaneng.2022.112122.

Lamonaca, F., Petris, G., Cianferra, M., Armenio, V., 2024. Non-reflective hard source method for multiple physically extended sources and scattering bodies. Phys. Fluids 36 (3), http://dx.doi.org/10.1063/5.0187929.

MacGillivray, A., de Jong, C., 2021. A reference spectrum model for estimating source levels of marine shipping based on automated identification system data. J. Mar. Sci. Eng. 9 (4), 369. http://dx.doi.org/10.3390/jmse9040369.

Marine Technology Centre (Coordinator, Spain), 2021. QUIETSEAS. URL https://quietseas.eu/.

Mendez, S., Shoeybi, M., Lele, S., Moin, P., 2013. On the use of the ffowcs williams-hawkings equation to predict far-field jet noise from large-eddy simulations. Int. J. Aeroacoustics 12 (1–2), 1–20. http://dx.doi.org/10.1260/1475-472X.12.1-2.1.

Petris, G., Cianferra, M., Armenio, V., 2022a. Marine propeller noise propagation within bounded domains. Ocean Eng. 265, 112618. http://dx.doi.org/10.1016/j.oceaneng.2022.112618.

Petris, G., Cianferra, M., Armenio, V., 2022b. A numerical method for the solution of the three-dimensional acoustic wave equation in a marine environment considering complex sources. Ocean Eng. 256, 111459. http://dx.doi.org/10.1016/j.oceaneng.2022.111459.

Posa, A., 2023. Comparison between the acoustic signatures of a conventional propeller and a tip-loaded propeller with winglets. Phys. Fluids 35 (2), http://dx.doi.org/10.1063/5.0136818.

Posa, A., Broglia, R., Felli, M., 2022a. Acoustic signature of a propeller operating upstream of a hydrofoil. Phys. Fluids 34 (6), http://dx.doi.org/10.1063/5.0096030.

Posa, A., Broglia, R., Felli, M., Cianferra, M., Armenio, V., 2022b. Hydroacoustic analysis of a marine propeller using large-eddy simulation and acoustic analogy. J. Fluid Mech. 947, A46. http://dx.doi.org/10.1017/jfm.2022.692.

Rijkswaterstaat (Coordinator, Netherlands), 2015. JOMOPANS - Joint Monitoring Programme for Ambient Noise North Sea. URL https://northsearegion.eu/jomopans.

Seol, H., Jung, B., Suh, J., Lee, S., 2002. Prediction of non-cavitating underwater propeller noise. J. Sound Vib. 257 (1), 131–156. http://dx.doi.org/10.1006/jsvi.2002.5035.

Stichting Netherlands Maritime Technology Foundation (Coordinator, Netherlands), 2012. SONIC - Suppression Of underwater Noise Induced by Cavitation. URL http://www.sonic-fp7.eu/.

Stichting Netherlands Maritime Technology Foundation (Coordinator, Netherlands), 2018. NAVAIS - New, Advanced and Value-Added Innovative Ships. URL https://www.navais.eu/.

Sturm, F., 2005. Numerical study of broadband sound pulse propagation in three-dimensional oceanic waveguides. J. Acoust. Soc. Am. 117 (3), 1058–1079. http://dx.doi.org/10.1121/1.1855791.

University College Cork – National University of Ireland, Cork (Coordinator, Ireland), 2019. JONAS - Joint Framework for Ocean Noise in the Atlantic Seas. URL http://www.jonasproject.eu/.

University College Cork – National University of Ireland, Cork (Coordinator, Ireland), 2021. SATURN - Solutions @ Underwater Radiated Noise. URL https://www.saturnh2020.eu/.

Wang, M., Freund, J.B., Lele, S.K., 2006. Computational prediction of flow-generated sound. Annu. Rev. Fluid Mech. 38, 483–512. http://dx.doi.org/10.1146/annurev.fluid.38.050304.092036.

Weinberg, H., Keenan, R.E., 1996. Gaussian ray bundles for modeling high-frequency propagation loss under shallow-water conditions. J. Acoust. Soc. Am. 100 (3), 1421–1431. http://dx.doi.org/10.1121/1.415989.